https://doi.org/10.5194/egusphere-2025-2301
Preprint. Discussion started: 10 June 2025


# Direct observation of core-shell structure and water uptake of individual submicron urban aerosol particles

Ruiqi Man[1], Yishu Zhu[1,†], Zhijun Wu[1,2,*], Peter Aaron Alpert[3,‡], Bingbing Wang[4], Jing Dou[5,§], Jie Chen[5], Yan Zheng[1], Yanli Ge[1], Qi Chen[1], Shiyi Chen[1], Xiangrui Kong[6], Markus Ammann[3], Min Hu[1]

[1]State Key Joint Laboratory of Environmental Simulation and Pollution Control, College of Environmental Sciences and Engineering, Peking University, Beijing, 100871, China

[2]Collaborative Innovation Center of Atmospheric Environment and Equipment Technology, Nanjing University of Information Science and Technology, Nanjing, 210044, China

[3]Laboratory of Atmospheric Chemistry, PSI Center for Energy and Environmental Sciences, Paul Scherrer Institute, Villigen, 5234, Switzerland

[4]College of Ocean and Earth Sciences, State Key Laboratory of Marine Environmental Science, Xiamen University, Xiamen, 361102, China

[5]Institute for Atmospheric and Climate Science, ETH Zürich, Zürich, 8092, Switzerland

[6]Department of Chemistry and Molecular Biology, University of Gothenburg, Gothenburg, 41390, Sweden

[†]now at Department of Earth and Planetary Science, University of California Berkeley, Berkeley, CA, 94720, USA

[‡]now at XRnanotech Gmbh, Parkstrasse 1, Villigen, 5234, Switzerland

[§]now at Institute for Atmospheric and Earth System Research, University of Helsinki, Helsinki, 00014, Finland

[*]*Correspondence to:* Zhijun Wu (zhijunwu@pku.edu.cn)

**Abstract.** Determining the particle chemical morphology is crucial for unraveling reactive uptake in atmospheric multiphase and heterogeneous chemistry. However, it remains challenging due to the complexity and inhomogeneity of aerosols particles. Using a scanning transmission X-ray microscopy (STXM) coupled with near-edge X-ray absorption fine structure (NEXAFS) spectroscopy and an environmental cell, we imaged and quantified the chemical morphology and hygroscopic behavior of individual submicron urban aerosol particles. Results show that internally mixed particles composed of organic carbon and inorganic matter (OCIn) dominated the particle population (73.1 ± 7.4%). At 86% relative humidity, 41.6% of the particles took up water, with OCIn particles constituting 76.8% of these hygroscopic particles. Most particles exhibited a core-shell structure under both dry and humid conditions, with an inorganic core and an organic shell. Our findings provide direct observational

https://doi.org/10.5194/egusphere-2025-2301
Preprint. Discussion started: 10 June 2025


evidence of the core-shell structure and water uptake behavior of typical urban aerosols, which underscore the importance of incorporating the core-shell structure into models for predicting the reactive uptake coefficient of heterogeneous reactions.

**Short summary:** The particle chemical morphology is important to atmospheric multiphase and heterogeneous chemistry. This work directly observed the core-shell structure and water uptake behavior of individual submicron aerosol particles at an urban site and elucidated the potential impact on particle reactive uptake and heterogeneous reactions.

**Keywords:** urban air pollution; individual particles; chemical morphology; core-shell structure; water uptake

**Table of Contents Graphic:**

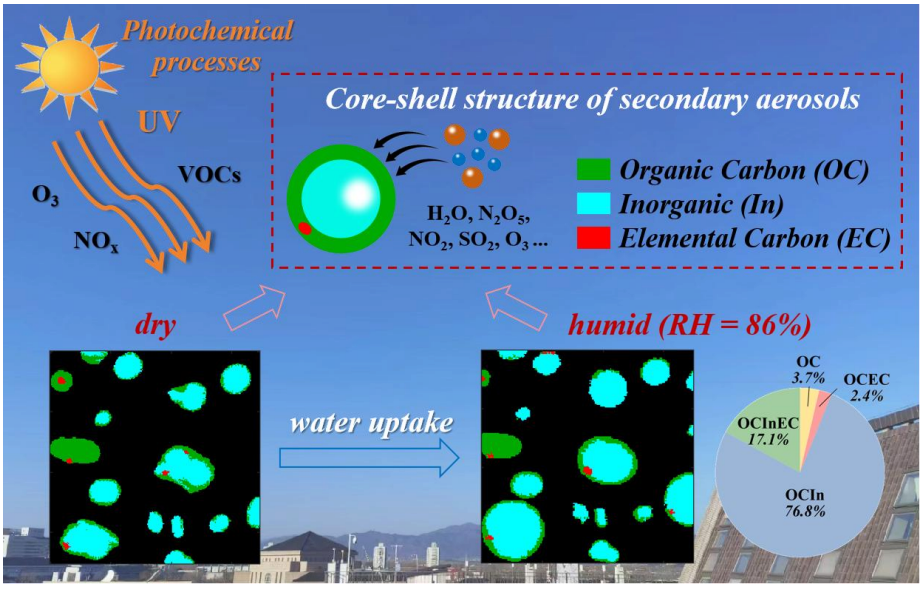

https://doi.org/10.5194/egusphere-2025-2301
Preprint. Discussion started: 10 June 2025


## 1 Introduction

Aerosols have significant impacts on visibility, climate, and human health (Mccormick and Ludwig, 1967; Noll et al., 1968; Chow et al., 2006; Rasool and Schneider, 1971). As particles in the atmosphere usually act as reaction vessels for various reactions, the physicochemical properties of aerosol particles play an important role in reactive uptake of gaseous molecules onto particles, mass transfer and gas-particle partitioning equilibrium, and transformation mechanisms of pollutants (Abbatt et al., 2012; Davidovits et al., 2011; George et al., 2015; George and Abbatt, 2010; Su et al., 2020; Ziemann and Atkinson, 2012). Therefore, quantitatively characterizing the aerosol physicochemical properties is vital to atmospheric multiphase and heterogeneous chemistry (Freedman, 2017; Li et al., 2016; Riemer et al., 2019; Tang et al., 2016).

The aerosol physicochemical properties, such as the particle size, chemical morphology (defined as the spatial distribution of various chemical components within a particle herein), mixing state, and hygroscopicity vary under different ambient conditions. These properties and their variations have a critical influence on reactive uptake, a key process in multiphase chemistry which is initiated by the collision of a gas-phase reactant with a condensed-phase surface (Davies and Wilson, 2018; Reynolds and Wilson, 2025). Organic coatings of particles with core-shell structures inhibit reactive uptake of dinitrogen pentoxide ($N_2O_5$) by particulate matter by means of affecting mass accommodation, the availability of water for hydrolysis, and mass transport (Wagner et al., 2013; Jahl et al., 2021; Jahn et al., 2021). Without considering the core-shell structure, the reactive uptake coefficient of $N_2O_5$ tends to be overestimated from several times to tens of times (Wagner et al., 2013). Therefore, investigating the particle chemical morphology is necessary for accurately quantifying the uptake coefficient and reducing uncertainty in heterogeneous reactions.

So far, extensive research has been conducted on the physicochemical properties of bulk aerosols by various techniques, such as the Humidified Tandem Differential Mobility Analyzer (H-TDMA), Aerosol Mass Spectrometer (AMS), and Soot Particle Aerosol Mass Spectrometer (SP-AMS) (Li et al., 2016; Tang et al., 2019; Riemer et al., 2019). However, the bulk analysis mostly obtains indirect information about the physicochemical properties of particle populations based on assumptions and estimations, which is difficult to directly observe the chemical morphology and mixing state of aerosol particles (Li et al., 2016). This knowledge gap hinders our understanding of the role of particle aerosols

https://doi.org/10.5194/egusphere-2025-2301
Preprint. Discussion started: 10 June 2025


in reactive uptake and heterogeneous processes. As a comparison, individual particle analysis can provide direct observational evidence about the chemical morphology and mixing state at the microscopic scale, which is essential for exploring particle hygroscopic and optical properties (Krieger et al., 2012; Li et al., 2016; Posfar et al., 2010; Wu and Ro, 2020).

Scanning transmission X-ray microscopy combined with near-edge X-ray absorption fine structure (STXM/NEXAFS) spectroscopy bases on synchrotron radiation technology. It is a robust technique for obtaining chemical morphology information of numerous individual particles with high spectral energy resolution, as it can resolve compositional contrast at the single particle level within a particle population. Compared with electron microscopy which is not well-suited for analyzing organic species, the soft X-ray energy range of STXM makes it possible to quantify light elements (such as C, N, O) with high chemical specificity, high spatial resolution, and little beam damage (Moffet et al., 2011; Shao et al., 2022). In addition, STXM doesn't require ultrahigh vacuum conditions. Therefore, STXM/NEXAFS spectroscopy has enormous potential in exploring ambient samples under atmospheric relevant conditions, especially submicron-sized particles.

Compared with other STXM which generally analyze samples under vacuum conditions (Alpert et al., 2022; Bondy et al., 2018; Fraund et al., 2020; Knopf et al., 2023; Lata et al., 2021; Moffet et al., 2010a; Moffet et al., 2010b; Moffet et al., 2013; Moffet et al., 2016; Tomlin et al., 2022), several STXM instruments are equipped with an in-situ temperature and relative humidity (RH) control environmental cell, allowing for investigating hygroscopicity and water uptake behavior of laboratory-generated particles (Ghorai and Tivanski, 2010; O'brien et al., 2015; Piens et al., 2016; Zelenay et al., 2011a; Zelenay et al., 2011b). However, only a few researches focusing on hygroscopic behavior of ambient particles has been reported so far, and these particles were collected in rural environment (Piens et al., 2016) or forest (Mikhailov et al., 2015; Pöhlker et al., 2014). Studies on water uptake of urban aerosol particles using STXM and corresponding knowledge for their chemical morphology under humid conditions is currently lacking.

In this study, we investigated the chemical morphology of ambient individual submicron aerosol particles using STXM/NEXAFS spectroscopy. The ambient samples were collected at an urban site in North China Plain during a pollution episode. We also explored the chemical morphology and water uptake behavior of individual particles at high humidity (RH = 86%) using an environmental cell. This work aims to improve our comprehension of the physicochemical properties of particles in typical

https://doi.org/10.5194/egusphere-2025-2301
Preprint. Discussion started: 10 June 2025


urban pollution atmospheres, aiding in clarifying their atmospheric heterogeneous processes and multiphase chemistry.

## 2 Materials and methods

### 2.1 Sampling and instruments

To study the physicochemical properties of ambient particles, samples were collected during a pollution episode at the Peking University Urban Atmosphere Environment Monitoring Station (PKUERS, 39°59′21″N, 116°18′25″E) in Beijing, China. More details about the measurement site can be found in our previous studies (Tang et al., 2021; Wu et al., 2007).

The individual particle sample was collected using a four-stage cascade impactor with a Leland Legacy personal sample pump (Sioutas, SKC, Inc., the US) at a flow rate of 9 L $min^{-1}$. The sampling started at 5:04 P.M. on October 1$^{st}$, 2019 and lasted for 5 minutes. The sampling substrate was a copper grid (Lacey Carbon 200 mesh, Ted Pella, Inc., the US) suitable for its X-ray transparency. Particles collected onto the last stage with the 50% cut-point aerodynamic diameter of 250-nm were used for STXM analysis. The sample was placed into a sample box sealed with a bag filled with nitrogen, and it was stored in a freezer at a temperature of –18°C until analysis.

Other parameters were measured from September 28$^{th}$ to October 7$^{th}$, 2019. The non-refractory chemical composition of submicron particles (NR-$PM_1$) was obtained by a Long Time-of-Flight Aerosol Mass Spectrometer (LTOF-AMS, Aerodyne Research Inc., the US) (Zheng et al., 2020; Zheng et al., 2023). Calibrations of ionization efficiency (IE) and relative IE followed the standard procedures described in previous studies (Canagaratna et al., 2007; Fröhlich et al., 2013). The reference temperature and pressure conditions of mass concentrations reported herein were 293.7 K and 101.82 KPa. We applied composition-dependent collection efficiency (CDCE) values (0.50 ± 0.01, mean ± standard deviation) that were calculated by the methods introduced by Middlebrook et al. (2012) to the AMS data. The mass concentration of fine particles ($PM_{2.5}$) was measured by a TEOM analyzer (TH-2000Z1, Wuhan Tianhong Environmental Protection Industry Co., Ltd., China). Meteorological parameters including temperature (*T*), RH, wind speed, and wind direction were monitored by an integrated 5-parameter Weather Station (MSO, Met One Instruments, Inc., the US).

https://doi.org/10.5194/egusphere-2025-2301
Preprint. Discussion started: 10 June 2025


### 2.2 STXM/NEXAFS analysis

In order to gain the chemical morphology, mixing state, and component information of individual particles, STXM/NEXAFS spectroscopy measurements were carried out at the PolLux beamline (X07DA) of the Swiss Light Source (SLS) at Paul Scherrer Institute (PSI) (Raabe et al., 2008). In brief, X-rays illuminated a Fresnel zone plate focusing the beam to a pixel of 35 × 35 $nm^2$. The zone plate has a central stop that acts together with another optic known as an order sorting aperture to eliminate unfocused and higher-order light, ensuring only first-order focused light is transmitted to the sample. Then, X-rays transmitted through the sample are detected. The absorbance of each pixel is characterized by optical density (OD) based on the Beer-Lambert's law as follows,

$$\mathrm{OD} = -\ln\left(I/I_0\right) \quad (1)$$

where $I$ and $I_0$ are the intensity of photons transmitted through a sample region and a sample-free region, respectively. Further details including the uncertainty estimation of OD are described in the Supplementary Information (SI).

STXM/NEXAFS spectroscopy scans X-ray energies over particles with high spectral energy resolution. When inner shell electrons of atoms absorb X-ray photons, they can transition into unoccupied valence orbitals, resulting in an absorption peak that is used to identify specific bonding characteristics. The amount of absorption depends on the photon energy ($E$), elemental composition, as well as sample thickness and density (Moffet et al., 2011). We employed two measurement strategies to optimize photon flux to the particles, achieving the best signal-to-noise ratio while minimizing the scan time. The first strategy was a high energy-resolution mode with an X-ray energy resolution $\Delta E$ = 0.2 eV and a coarse pixel size of around 100 × 100 $nm^2$ to measure absorption at small energy steps. The energy resolution is defined as being able to distinguish between two absorption peaks separated by $\Delta E$ at the full width at half maximum OD. In this mode, carbon (C), nitrogen (N), and oxygen (O) K-edge spectra of individual particles were measured. The energy offset of C and O spectra were +0.4 eV and +1.2 eV respectively, according to the energy calibration procedures using polystyrene spheres and gas-phase carbon dioxide ($CO_2$). The energy offset of N at the K-edge was not calibrated, however, the obtained spectra of ambient particles appeared identical to ammonium salts in literatures (Ekimova et al., 2017; Latham et al., 2017). Due to the presence of ammonium, which was confirmed in particles

https://doi.org/10.5194/egusphere-2025-2301
Preprint. Discussion started: 10 June 2025


using AMS, we applied a calibration factor of +0.1 eV for the N K-edge to match our observed main peak to that of ammonium at 405.7 eV.

The second strategy is a high spatial-resolution mode with a pixel size of 35 × 35 $nm^2$ and $\Delta E$ = 0.6 eV, where imaged at four specific energies for the C K-edge, namely, 278.0 eV, 285.4 eV, 288.6 eV, and 320.0 eV. Automated analysis followed the methodology of Moffet et al. (2010a). In brief, absorption at 278.0 eV ($OD_{278.0eV}$) is regarded as the pre-edge of carbon, which is mainly due to off-resonance absorption by inorganic elements other than carbon. Absorption at 285.4 eV ($OD_{285.4eV}$) is due to the characteristic transition of $sp^2$ hybridized carbon (i.e., doubly bonded carbon). Since this peak is abundant for elemental carbon (EC), it can be used to discern soot, because EC is a type of components of soot (Penner and Novakov, 1996). Absorption at 288.5 eV ($OD_{288.5eV}$) comes from carboxylic carbonyl groups, which are common in organic aerosols in atmospheres. Therefore, organic carbon (OC) is identified by this energy. Absorption of the post-edge at 320.0 eV ($OD_{320.0eV}$) is contributed by carbonaceous and non-carbonaceous atoms (Moffet et al., 2010a).

Based on absorption at these four typical energies, we obtain three images by further processing. The difference between OD at the post-edge and OD at the pre-edge ($OD_{320.0eV}$ - $OD_{278.0eV}$) indicates total carbon. The ratio of OD at the pre-edge to OD at the post-edge ($OD_{278.0eV}$ / $OD_{320.0eV}$) indicates the relative absorption contribution of inorganic matter (In). Compared with the absorbance contribution of doubly bonded carbon to total carbon (%$sp^2$) in the highly oriented polycrystalline graphite (HOPG, assuming that %$sp^2$ = 100%) at 285.4 eV, the spatial distribution of EC/soot in samples can be identified by the procedure of Hopkins et al. (2007). It is assumed that total carbon consists of OC and EC. These three images described above were then overlaid to create a chemical map of individual particles.

### 2.3 Criterion of particle water uptake based on the total oxygen absorbance

To determine whether particles took up water, a criterion was established on the basis of the total oxygen absorbance determined at the energy of 525.0 eV (the pre-edge of oxygen) and 550.0 eV (the post-edge of oxygen). Based on the same principle as the total carbon calculation, the difference between OD at the post-edge and pre-edge of oxygen represents the total oxygen absorbance. Due to the fact that each particle is composed of some pixels, the total oxygen absorbance (ΔOD) of an individual particle under dry and humid conditions is calculated as follows,

https://doi.org/10.5194/egusphere-2025-2301
Preprint. Discussion started: 10 June 2025


$$\Delta OD_{dry} = \sum_{i=1}^{m} \Delta OD_i = \sum_{i=1}^{m} (OD_{post,i} - OD_{pre,i}) = \sum_{i=1}^{m} OD_{post,i} - \sum_{i=1}^{m} OD_{pre,i} \quad (2)$$

$$\Delta OD_{humid} = \sum_{j=1}^{n} \Delta OD_j = \sum_{j=1}^{n} (OD_{post,j} - OD_{pre,j}) = \sum_{j=1}^{n} OD_{post,j} - \sum_{j=1}^{n} OD_{pre,j} \quad (3)$$

where $m$ and $n$ are numbers of pixels that make up an individual particle under dry and humid conditions, $i$ and $j$ are a certain pixel within an individual particle under dry and humid conditions, *post* and *pre* respectively represent the energy at the post-edge (550.0 eV) and that at the pre-edge (525.0 eV) of oxygen. If a particle takes up water, the amount of oxygen atoms within this particle will increase, leading to an amplification in ΔOD. Water uptake may increase particle height and absorption. On the other hand, it possibly causes a particle to spread out, which may reduce particle height and thus absorption. Although a thinner particle that contains more water may result in less absorption at some specific pixels, $\Delta OD_{humid}$ will be larger than $\Delta OD_{dry}$ due to the fact that more pixels are summed, i.e., $n > m$. Therefore, comparing the results of Eq. 2 and Eq. 3 will quantify the total oxygen absorbance of a particle under dry and humid conditions, and determine particle water uptake. Specifically, if $\Delta OD_{humid} > \Delta OD_{dry}$, then we assume that the particle has taken up water.

### 2.4 A novel in-situ environmental cell

To explore the chemical morphology and hygroscopicity of the particles under humid conditions, we adjusted the RH of an in-situ environmental cell with sample placed in it. The environmental cell can also be used for trace gas reactive uptake and photochemical reactions with laboratory-generated particles (Alpert et al., 2019; Alpert et al., 2021). The environmental cell used in this study consists of a removable sample clip that hosts a sealed silicon nitride (SiNit) window and a main body that contains gas supply lines and temperature control. Together, they are mounted in the STXM vacuum chamber. A SiNit window at the back side of the main body is also sealed and ensures X-ray transparency passing through the whole environmental cell assembly. Descriptions of the connections for the gas supply, heating and cooling devices, and temperature measurement can be found in previous studies (Huthwelker et al., 2010; Zelenay et al., 2011a). The detailed methods of collecting the ambient particles by the impactor and measuring them in the environmental cell were shown in the SI.

We performed humidity calibration experiments to make sure sufficient heat transfer and a homogeneous water vapor field across the samples. It is important due to the fact that the only way for

https://doi.org/10.5194/egusphere-2025-2301
Preprint. Discussion started: 10 June 2025


samples to gain or lose heat and water was through air contact. To study the accuracy of RH in the environmental cell, water uptake and deliquescence of a sodium chloride (NaCl) standard sample was observed. The deliquescence relative humidity (DRH) of pure NaCl crystals obtained from literatures and thermodynamic models is around 75 – 76% at room temperature (Eom et al., 2014; Martin, 2000; Peng et al., 2022). The images of the NaCl sample displayed in Fig. S1 illustrate the morphological changes as RH increased. As shown in Fig. S1, particle morphologies in panels (A) – (C) remained essentially identical before RH reached the DRH of NaCl, although the focus position slightly varied in different panels. When RH was 75.6% (Fig. S1D), particles completely deliquesced and some coalesced. The uncertainty of RH in the environmental cell in this study was determined conservatively to be ±2%, in agreement with previous results (Huthwelker et al., 2010). Information about the oxygen K-edge spectra of the NaCl sample at high RH can be found in Fig. S2.

## 3 Results and discussion

### 3.1 Pollution characteristics during the sampling period

Time series of meteorological parameters, mass concentrations of gaseous pollutants, $PM_{2.5}$, and NR-$PM_1$ are shown in Fig. 1. During the pollution episode from September 29$^{th}$ to October 3$^{rd}$, 2019, the stagnant weather condition with low wind speed led to pollution accumulation. The air became clean due to the appearance of a strong north wind on October 4$^{th}$ (Fig. 1A). The sampling time of the individual particle sample was 5:04 P.M. on October 1$^{st}$ (see the red line in Fig. 1) with an ozone ($O_3$) concentration of 97.1 ppb. At that time, the low mass fraction of volatile inorganic species such as nitrate made it suitable for measurements using offline techniques, such as STXM, because the loss of volatile species during storage and measurement processes was minimal.

During the pollution episode, the maximum daily 8-hour average of ozone (MDA8-$O_3$) was 110.3 ± 10.1 ppb (i.e., 236.5 ± 21.7 μg m$^{-3}$). The concentration of $O_x$ [$O_x$ = nitrogen dioxide ($NO_2$) + $O_3$] was 88.6 ± 29.4 ppb (Fig. 1B), reflecting a high atmospheric oxidation capacity that drives secondary transformations of gaseous pollutants (Dou et al., 2024; Xiao et al., 2022). The average $PM_{2.5}$ was 74.3 ± 18.3 μg m$^{-3}$ (Fig. 1C). As shown in Fig. 1D – 1E, the average mass concentration of secondary inorganic aerosol (SIA) in NR-$PM_1$ was 21.3 ± 4.8 μg m$^{-3}$, with sulfate and nitrate contributing almost equally to particle mass (i.e., 18.1% and 17.3% respectively). Organic matter in NR-$PM_1$ had an

https://doi.org/10.5194/egusphere-2025-2301
Preprint. Discussion started: 10 June 2025


239 average mass fraction of 56.4% (Fig. 1E). The mass concentrations of primary organic aerosol (POA)
240 and secondary organic aerosol (SOA) were estimated based on the positive matrix factorization (PMF)
241 analysis (Ulbrich et al., 2009). As shown in Fig. 1F, SOA dominated organic matter, contributing an
242 average of 68.9%. Overall, this pollution episode was led by secondary oxidation processes and
243 featured by high contributions of secondary particulate species.

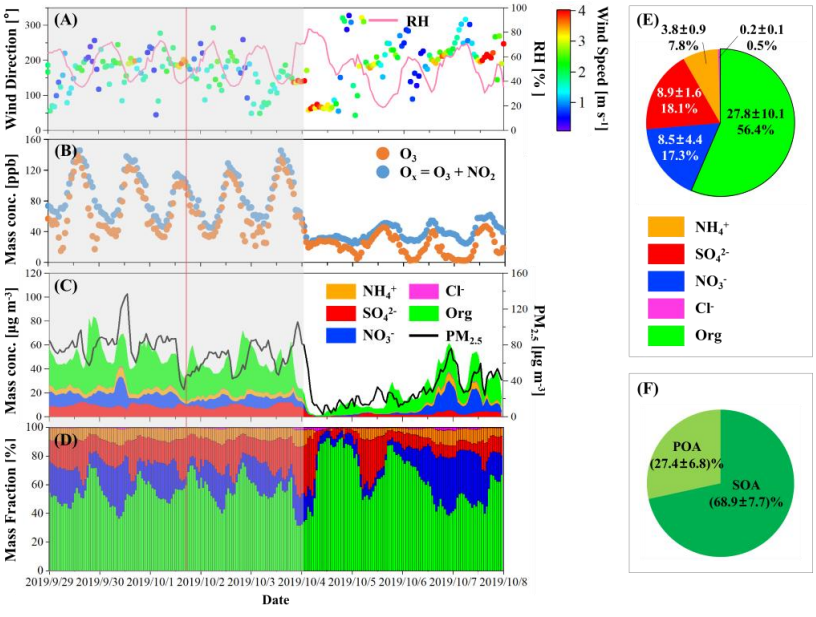


244

245 **Figure 1: Time series of (A) wind direction, wind speed, and relative humidity (RH), (B) mass**
246 **concentrations of ozone ($O_3$) and $O_x$ ($O_3$ + nitrogen dioxide, $NO_2$), (C) mass concentrations of fine particles**
247 **($PM_{2.5}$) and non-refractory submicron particles (NR-$PM_1$), and (D) mass fractions of chemical composition**
248 **of NR-$PM_1$ are shown. The gray area represents the pollution episode lasting from September 29th to**
249 **October 3rd. The red line indicates the sampling time for the individual particle sample. (E) Pie chart**
250 **showing the average mass fractions of chemical composition of NR-$PM_1$ during the pollution period. The**
251 **number in the first row of each part is the average mass concentration and standard deviation (SD) with a**
252 **unit of μg $m^{-3}$. The number in the second row is the average mass fraction. (F) Pie chart showing the**
253 **average mass contributions of primary organic aerosol (POA, light green) and secondary organic aerosol**
254 **(SOA, dark green) to the total organic. Average mass fraction and SD are marked in the pie chart.**

255 **3.2 Chemical maps of individual particles**

256 Chemical maps of individual particles under dry conditions are displayed in Fig. 2. Different
257 images denote particles located in different regions of interest (ROI, 12 in total) of the sampling
258 substrate. 197 individual particles were investigated in total. Detailed images of total carbon, inorganic,
259 and doubly bonded carbon maps are available in the SI (Fig. S3 – S5). Most submicron particles on the

https://doi.org/10.5194/egusphere-2025-2301
Preprint. Discussion started: 10 June 2025


substrate were round or nearly round, while supermicron particles predominantly exhibited irregular shapes. The circular equivalent diameter of individual particles was calculated, with the methods detailed in the SI. The normalized size distribution of overall particles followed a normal distribution, with a mean diameter ± standard deviation (SD) being 0.83 ± 0.30 μm (Fig. S6A). A significant proportion of the particles were within the 0.4 – 1.2 μm size range.

As displayed in Fig. 2, chemical maps of individual particles showed that they were dominated by inorganic substances (colored in cyan), which were likely sulfate that was frequently observed by AMS (Fig. 1C). Approximately one quarter (24.9%) of the particles contained EC/soot (colored in red), found either near the center or at the edge of individual particles. Notably, around 82% of these soot-containing particles had soot located at particle edges. The possible reason is that inorganic species (such as crystals) pushed soot away from the center of the particles during their efflorescence (Moffet et al., 2016). The morphology of soot varied, showing fractal or compact structures of various sizes. Additionally, several particles contained multiple soot components, which was also observed before (Moffet et al., 2016).

Typically, inorganic components and/or soot were encased in organic matter, forming a core-shell structure characterized by an inorganic-dominated core and an organic-dominated shell. Figure 2 illustrates that most organic-inorganic internally mixed particles exhibited thin coatings, likely from fresh emissions. Conversely, a few particles have thick coatings, which is indicative of aging processes in a highly active photochemical environment. Previous studies suggest that most of the soot-containing particles with thin coatings would have rather smaller absorption enhancement compared with those with thick coatings (Bond et al., 2006; Moffet et al., 2016).

The observed core-shell morphology could also result from liquid-liquid phase separation (LLPS), influenced by fluctuating ambient RH (Fig. 1A) and determined by the oxygen-to-carbon (O:C) ratio of the organic fraction (Freedman, 2020; Li et al., 2021; You et al., 2012; You et al., 2014; Freedman, 2017). To test this hypothesis, the O:C ratio of individual particles composed of pure organic composition was estimated as 0.53 ± 0.15 based on the STXM data. The estimation methods were displayed in the SI. This falls within the threshold range for LLPS occurrence in ammonium sulfate - organic mixing particles ($0 < O:C < 0.57$) (You et al., 2013).

https://doi.org/10.5194/egusphere-2025-2301
Preprint. Discussion started: 10 June 2025


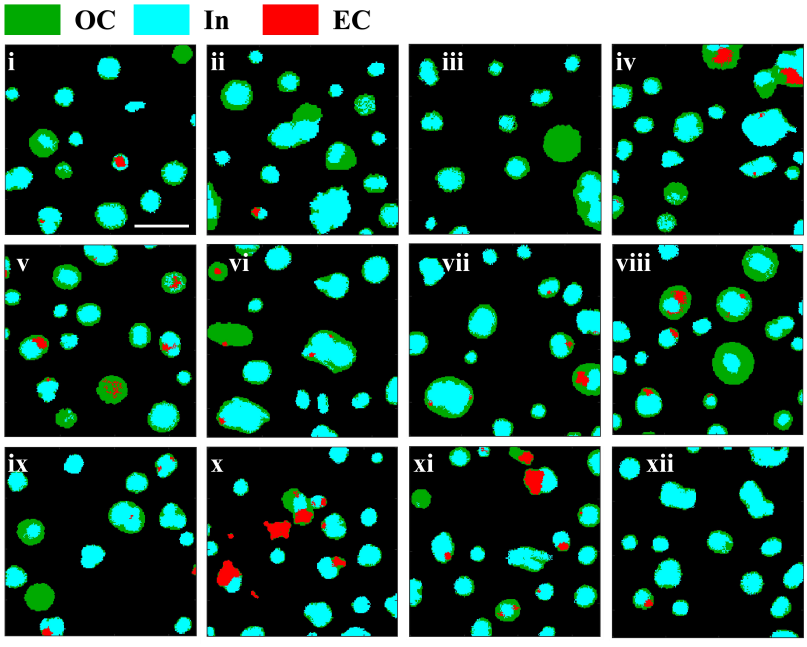


**Figure 2: Chemical maps of individual particles in 12 regions of interest (ROI) of sampling substrate under dry conditions on the basis of pixels. Green, cyan, and red color represent dominant components of organic carbon (OC), inorganic matter (In), and elemental carbon (EC), respectively. The scale bar in the upper left image represents 2 μm and applies to all images.**

Statistically, the particles were categorized into four types based on their mixing state, including pure organic (OC), organic internally mixed with soot (OCEC), organic internally mixed with inorganic (OCIn), and organic internally mixed with inorganic and soot (OCInEC). OCIn particles were the most abundant type in the examined particle population (73.1 ± 7.4%), followed by OCInEC (20.8 ± 6.7%) and OCEC (4.1 ± 3.3%), indicating a highly internally mixed particle population. Pure organic particles only accounted for 2.0 ± 2.3%. The calculation of the margin of error of the mixing state proportions can be found in the SI. The mean diameters of OCEC, OCIn, and OCInEC particles were 0.66, 0.79, and 1.02 μm, respectively (Fig. S7). This suggests that the internally mixed particles containing three species families tend to be larger than those composed of two species families.

### 3.3 The effects of particle water uptake on chemical maps

Chemical maps of individual particles under humid conditions (RH = 86%) measured in the environmental cell were displayed in Fig. 3, and these ROI are identical and matched one by one to

https://doi.org/10.5194/egusphere-2025-2301
Preprint. Discussion started: 10 June 2025


those in Fig. 2. It was observed that many particles tended to be more rounded due to water uptake at high RH, especially for particles with diameters in the supermicron range (e.g., particles in (ii), (vi), (xi), and (xii) in Fig. 3). If particles take up significant amounts of water and are homogeneously mixed, they would appear as dominated by inorganic (colored in cyan) due to absorption of a large amount of water at the carbon pre-edge. In contrast, most particles remained inhomogeneous and exhibited a core-shell structure under humid conditions. A possible reason is that the settled RH may not reach the mixing relative humidity (MRH) of particles, which is defined as a threshold where different phases in an aqueous particle mix into one homogeneous phase. This MRH usually varies from 84% to over 90% (Li et al., 2021; You et al., 2014; Zhang et al., 2022).

Additionally, around 87% of soot was located at the edge of the humidified particles, with no obvious location change of soot observed in most particles. This phenomenon aligns with a previous study which indicates that the phase transition of phase-separated particles without phase mixing will not cause the redistribution of soot within individual particles (Zhang et al., 2022).

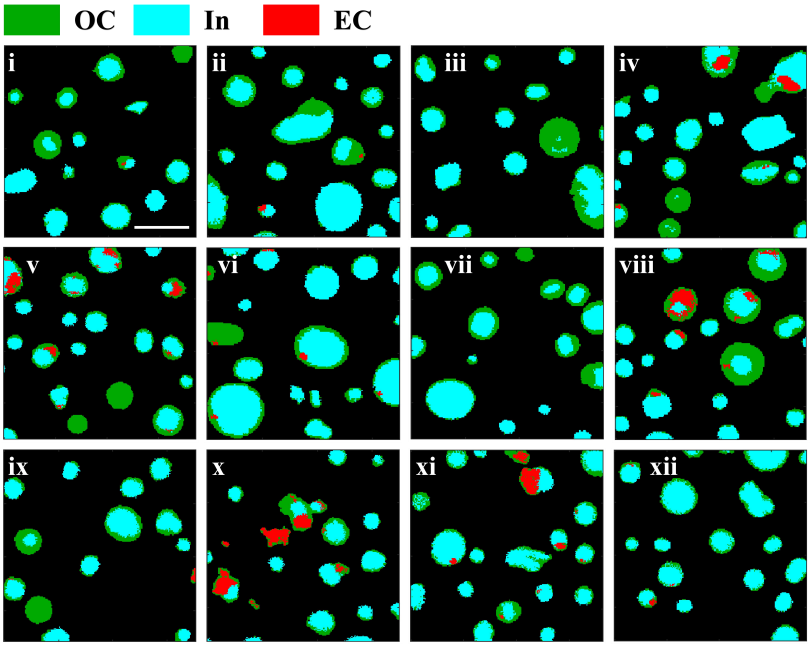


**Figure 3: Chemical maps of individual particles in 12 ROI of sampling substrate under humid conditions (RH = 86%) measured in an in-situ environmental cell. Green, cyan, and red color represent dominant components of OC, In, and EC, respectively. The scale bar in the upper left image represents 2 μm and applied to all images.**

https://doi.org/10.5194/egusphere-2025-2301
Preprint. Discussion started: 10 June 2025


Comparing size distributions of particle populations under dry (Fig. S6A) and humid conditions (Fig. S6B) reveals that they exhibited similar distribution characteristics. The mean diameter of overall particles at high RH was 0.86 ± 0.33 μm, compared with 0.83 ± 0.30 μm under dry conditions. This indicates that the overall size distribution of the humidified particles shifted a little towards larger particles due to water uptake. Specifically, approximately 56.3% of the particles showed an average increase of 14.9% in diameter, while the remaining exhibited an average decrease of 8.2%. Pöhlker et al. (2014) also observed this abnormal phenomenon where some particles decreased in size with increasing RH. They suggested that it could be attributed to the decreasing viscosity and increasing surface tension due to particle water uptake at high RH. This led to larger contact angles between the collected particles and the substrate, causing the particles to 'bead up' and therefore reducing their cross-section areas in the view (Pöhlker et al., 2014). In addition, one should note that a small number of particles at the edge of the ROI did not entirely enter the field of view due to the limited observation range, which may slightly affect the quantification of their size.

According to the criterion for water uptake by individual particles based on the total oxygen absorbance described in the Sect. 2.3, 41.6% of the particles took up water. As shown in Fig. S8A, OCIn particles were the dominant mixing state type taking up water (76.8%), followed by OCInEC (17.1%). There were also several OCEC (2.4%) and OC (3.7%) particles displayed water uptake. Different particle mixing state types exhibited distinct patterns of hygroscopic behavior. For instance, 43.8% of OCIn particles took up water, while 34.1% of OCInEC particles performed the same. This difference may be attributed to the varying hygroscopicity of different components. For example, the single hygroscopic parameter (κ) of ammonium nitrate, ammonium sulfate, ammonium hydrogen sulfate, POA, and SOA is 0.58, 0.48, 0.56, 0, and 0.1, respectively (Wu et al., 2016). Based on the AMS data, κ of bulk aerosols during the sampling period (0.25 ± 0.01) was calculated according to the Zdanovskii-Stokes-Robinson (ZSR) mixing rule (Stokes and Robinson, 1966), indicating a relatively low hygroscopic capacity of NR-$PM_1$ during sampling, which could explain why only less than half of the particles exhibited water uptake at such high humidity conditions. In addition, the average diameter of particles taking up water increased from 0.82 ± 0.33 μm to 0.91 ± 0.36 μm. The relative frequency distribution and the size-resolved fraction of particles taking up water can be found in Fig. S8B.

https://doi.org/10.5194/egusphere-2025-2301
Preprint. Discussion started: 10 June 2025


### 3.4 Chemical composition of ambient submicron particles

NEXAFS spectra with high energy resolution were measured at the C (278 – 320 eV), N (395 – 430 eV), and O (525 – 550 eV) K-edges. As shown in Fig. 4A, three notable absorption peaks at the C K-edge were observed at 285.4, 286.7, and 288.6 eV. According to previous literatures (Warwick et al., 1998; Moffet et al., 2010a), the peak at 285.4 eV refers to the characteristic transition of $sp^2$ hybridized carbon (C 1s→$\pi^*_{R(C^*=C)R}$). The peak at 286.7 eV may result from the transition of ketonic carbonyl (C 1s→$\pi^*_{R(C^*=O)R}$), representing ketone and ketone-like compounds. The peak appearing at 288.6 eV represents the characteristic transition of carboxylic carbonyl functional groups (C 1s→$\pi^*_{R(C^*=O)OH}$), which refers to organic matter and is always found in the outer shell of particles (Moffet et al., 2016; Prather et al., 2013). In addition, two other peaks at 296.8 and 299.6 eV were present (see spectra (d) and (e) in Fig. 4A), corresponding to the $L_2$- and $L_3$-edges of potassium (K) (Moffet et al., 2010a). In our sample, K may come from biomass burning processes based on a previous study (Wu et al., 2017).

Nitrogen K-edge spectra in Fig. 4B illustrate that ammonium salts were the main nitrogen species in the sample. We observed a broad main peak centered at 405.7 eV, which is the feature of ammonium (Ekimova et al., 2017). A smaller peak was observed at 401.0 eV, which is absorption due to nitrogen gas ($N_2$) either trapped in the inorganic crystal or formed under X-ray exposure (Latham et al., 2017). Absorption of nitrate ($NO_3^-$) and nitrite ($NO_2^-$) commonly have narrow peaks at 405.1 eV and 401.7 eV (Smith et al., 2015), respectively, which were not apparent in our spectra. This is likely because particulate nitrite is below the detection limit, or its peak is masked by the pronounced absorption of ammonium ($NH_4^+$). The solid ammonium nitrate and sodium nitrate salts could exhibit a peak at around 415.0 eV (Smith et al., 2015). However, this was not observed in Fig. 4B. Organic compounds containing nitrogen, such as amino acids, N-heterocyclics, and nitroaromatic compounds, can be abundant in urban aerosol particles due to combustion sources (Yu et al., 2024). They have a large variety of possible peak positions, heights, and widths (Leinweber et al., 2007), making the identification of these compounds difficult. Although a positive identification of specific organic nitrides cannot be made, we note that amino acids and 5- or 6-ring heterocycles commonly have narrow peaks at around 401 eV and broad peaks at 405 eV (Leinweber et al., 2007). We expect that organic nitrides did contribute to the observed N K-edge spectra, although a targeted study on molecular identification would be necessary to establish further certainty.

https://doi.org/10.5194/egusphere-2025-2301
Preprint. Discussion started: 10 June 2025


Oxygen K-edge spectra in Fig. 4C exhibited a large peak at 536.9 eV, which is a representative characteristic of sulfate-rich particles, consistent with the result of AMS. A smaller peak was observed at 532.5 eV, confirming the presence of ketone, aldehyde, or carboxyl functionalities (Colberg et al., 2004; Slowik et al., 2011; Mikhailov et al., 2015; Pöhlker et al., 2014), which aligns with the results from C K-edge spectra. These compositions tend to take up water under humid conditions.

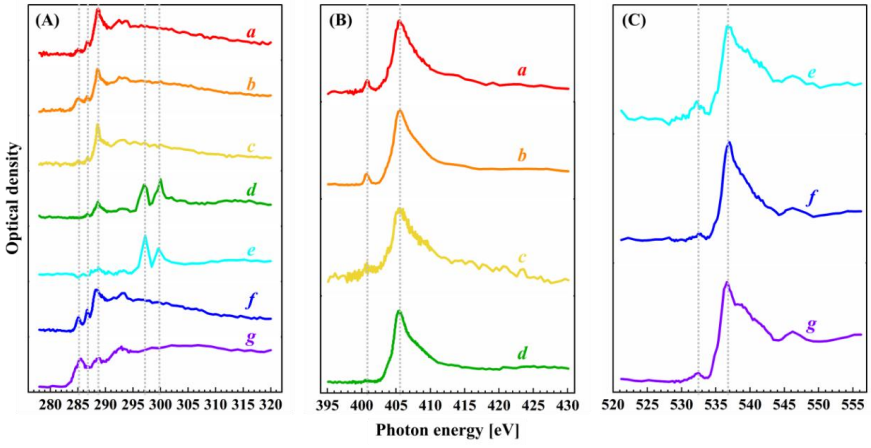


**Figure 4: NEXAFS spectra for individual particles at (A) carbon (C), (B) nitrogen (N), and (C) oxygen (O) K-edges. In panel (A), peaks were observed at 285.4, 286.7, and 288.6 eV, and two typical peaks appeared at around 296.8 and 299.6 eV in spectra (d) and (e). In panel (B), a main peak appeared at 405.7 eV, and a smaller peak appeared at 410.0 eV. In panel (C), a main peak appeared at 536.9 eV, and a smaller peak was at 532.5 eV. Each small case letter of a spectrum stands for the average result of all the pixels within an individual particle. The same letter in different panels doesn't refer to a same particle.**

## 4 Conclusions and implications

Particles in the atmosphere usually act as reaction vessels for heterogeneous reactive uptake of gaseous molecules, which play an important part in gas-particle partitioning and secondary aerosol formation (Abbatt et al., 2012; Davidovits et al., 2011; Kolb et al., 2010). However, determining the particle physicochemical properties is crucial but challenging due to the complexity and inhomogeneity of aerosols particles (Barbaray et al., 1979; Zong et al., 2022). So far, there is a lack of study on direct observation of the physicochemical properties of urban aerosols at the single particle level under different conditions, which hinders our understanding of the role of urban particle aerosols in multiphase and heterogeneous chemistry.

In this study, we used STXM/NEXAFS spectroscopy combined with an environmental cell to

https://doi.org/10.5194/egusphere-2025-2301
Preprint. Discussion started: 10 June 2025


image and quantify the chemical morphology and water uptake behavior of individual submicron particles collected in an urban pollution atmosphere. Results show that most organic compounds were internally mixed with inorganic and/or soot, generally presenting a core-shell structure with an inorganic core and an organic shell. Internally mixed particles composed of organic carbon and inorganic matter dominated the particle population by 73.1 ± 7.4%. At 86%RH, 41.6% of the particles took up water, with OCIn particles making up 76.8% of these hygroscopic particles. The relatively low hygroscopicity of bulk aerosols during the sampling period ($\kappa$ = 0.25 ± 0.01) helps to explain the reason why only less than half of the particles took up water. Besides, the majority of particles still showed a heterogeneous core-shell morphology under humid conditions.

This study directly displays the dominant chemical morphology (i.e., core-shell structure) and hygroscopic behavior of individual submicron urban aerosol particles at the microscale. Results highlight the importance of taking the core-shell structure into consideration for estimating the uptake coefficient and investigating heterogeneous reactions, which can improve our comprehension of atmospheric processes of secondary aerosols in typical urban pollution atmospheres. Moreover, previous studies found that the impact of organics on the reactive uptake coefficient mainly relies on organic species, organic content, and particle mixing state (Wagner et al., 2013). Therefore, it is instrumental to conduct research on the basis of organic molecules and functional groups in further study.

https://doi.org/10.5194/egusphere-2025-2301
Preprint. Discussion started: 10 June 2025


## ASSOCIATED CONTENT

***Data availability.*** The data presented in this article can be accessed through the corresponding author Zhijun Wu via E-mail (zhijunwu@pku.edu.cn).

***Author contributions.*** YSZ, PAA, BBW, and JD measured the individual particle sample by STXM/NEXAFS. YSZ, ZJW, YZ, YLG, QC, and SYC carried out the field observation and obtained data. RQM and PAA processed and analyzed data. All authors discussed the results and contributed to the writing of this paper. RQM prepared the manuscript. ZJW, PAA, JC, XRK, MA, and MH further modified and improved the manuscript.

***Competing Interests.*** The authors declare that they have no conflict of interest.

***Acknowledgements.*** We gratefully acknowledge the Swiss Light Source (SLS) for providing a platform for sample measurements. We also thank Benjamin Watts for helping us dealing with technical problems about STXM/NEXAFS.

***Financial support.*** This work has been supported by National Natural Science Foundation of China, International (Regional) Cooperation and Communication Project (NSFC-STINT, China and Sweden; grant No. 42011530121), NSFC (No. 41775133), and the SNSF Swiss Postdoctoral Fellowships (SPF, grant TMPFP2_209830).

https://doi.org/10.5194/egusphere-2025-2301
Preprint. Discussion started: 10 June 2025


436 **References**

437 Abbatt, J. P. D., Lee, A. K. Y., and Thornton, J. A.: Quantifying trace gas uptake to tropospheric
438 aerosol: recent advances and remaining challenges, Chem. Soc. Rev., 41, 6555–6581, DOI:
439 10.1039/c2cs35052a, 2012.
440 Alpert, P. A., Arroyo, P. C., Dou, J., Krieger, U. K., Steimer, S. S., Förster, J.-D., Ditas, F., Pöhlker, C.,
441 Rossignol, S., Passananti, M., Perrier, S., George, C., Shiraiwa, M., Berkemeier, T., Watts, B., and
442 Ammann, M.: Visualizing reaction and diffusion in xanthan gum aerosol particles exposed to
443 ozone, Phys. Chem. Chem. Phys., 21, 20613–20627, DOI: 10.1039/c9cp03731d, 2019.
444 Alpert, P. A., Dou, J., Arroyo, P. C., Schneider, F., Xto, J., Luo, B. P., Peter, T., Huthwelker, T., Borca,
445 C. N., Henzler, K. D., Schaefer, T., Herrmann, H., Raabe, J., Watts, B., Krieger, U. K., and
446 Ammann, M.: Photolytic radical persistence due to anoxia in viscous aerosol particles, Nat.
447 Commun., 12, 1769, DOI: 10.1038/s41467-021-21913-x, 2021.
448 Alpert, P. A., Kilthau, W. P., O'Brien, R. E., Moffet, R. C., Gilles, M. K., Wang, B. B., Laskin, A.,
449 Aller, J. Y., and Knopf, D. A.: Ice-nucleating agents in sea spray aerosol identified and quantified
450 with a holistic multimodal freezing model, Sci. Adv., 8, eabq6842, DOI: 10.1126/sciadv.abq6842,
451 2022.
452 Barbaray, B., Contour, J. P., Mouvier, G., Barde, R., Maffiolo, G., and Millancourt, B.: Chemical
453 heterogeneity of aerosol samples as revealed by atomic absorption and x-ray photoelectron
454 spectroscopy, Environ. Sci. Technol., 13, 1530–1532, DOI: 10.1021/es60160a008, 1979.
455 Bond, T. C., Habib, G., and Bergstrom, R. W.: Limitations in the enhancement of visible light
456 absorption due to mixing state, J. Geophys. Res.: Atmos., 111, D20211, DOI:
457 10.1029/2006jd007315, 2006.
458 Bondy, A. L., Bonanno, D., Moffet, R. C., Wang, B. B., Laskin, A., and Ault, A. P.: The diverse
459 chemical mixing state of aerosol particles in the southeastern United States, Atmos. Chem. Phys.,
460 18, 12595–12612, DOI: 10.5194/acp-18-12595-2018, 2018.
461 Canagaratna, M. R., Jayne, J. T., Jimenez, J. L., Allan, J. D., Alfarra, M. R., Zhang, Q., Onasch, T. B.,
462 Drewnick, F., Coe, H., Middlebrook, A., Delia, A., Williams, L. R., Trimborn, A. M., Northway,
463 M. J., DeCarlo, P. F., Kolb, C. E., Davidovits, P., and Worsnop, D. R.: Chemical and
464 microphysical characterization of ambient aerosols with the aerodyne aerosol mass spectrometer,
465 Mass Spectrom. Rev., 26, 185–222, 10.1002/mas.20115, 2007.

https://doi.org/10.5194/egusphere-2025-2301
Preprint. Discussion started: 10 June 2025


466 Chow, J. C., Watson, J. G., Mauderly, J. L., Costa, D.L., Wyzga, R.E., Vedal, S., Hidy, G. M.,
467 Altshuler, S. L., Marrack, D., Heuss, J. M., Wolff, G. T., Pope, C. A., and Dockery, D. W.: Health
468 effects of fine particulate air pollution: Lines that connect, J. Air Waste Manage. Assoc., 56,
469 1368–1380, DOI: 10.1080/10473289.2006.10464545, 2006.
470 Colberg, C. A., Krieger, U. K., and Peter, T.: Morphological investigations of single levitated
471 $H_2SO_4/NH_3/H_2O$ aerosol particles during deliquescence/efflorescence experiments, J. Phys. Chem.
472 A., 108, 2700–2709, DOI: 10.1021/jp037628r, 2004.
473 Davidovits, P., Kolb, C. E., Williams, L. R., Jayne, J. T., and Worsnop, D. R.: Update 1 of: Mass
474 Accommodation and Chemical Reactions at Gas-Liquid Interfaces, Chem. Rev., 111,
475 PR76–PR109, DOI: 10.1021/cr100360b, 2011.
476 Davies, J. F. and Wilson, K. R.: Chapter 13 - Heterogeneous Reactions in Aerosol, Physical Chemistry
477 of Gas-Liquid Interfaces, edited by: Faust, J. A. and House, J. E., Elsevier, the Netherlands,
478 403–433, ISBN: 9780128136416, 2018.
479 Dou, X. D., Yu, S. C., Li, J. L., Sun, Y. H., Song, Z., Yao, N. N., and Li, P. F.: The WRF-CMAQ
480 Simulation of a Complex Pollution Episode with High-Level $O_3$ and $PM_{2.5}$ over the North China
481 Plain: Pollution Characteristics and Causes, Atmosphere, 15, 198, DOI: 10.3390/atmos15020198,
482 2024.
483 Ekimova, M., Quevedo, W., Szyc, L., Iannuzzi, M., Wernet, P., Odelius, M., and Nibbering, E. T. J.:
484 Aqueous Solvation of Ammonia and Ammonium: Probing Hydrogen Bond Motifs with FT-IR and
485 Soft X-ray Spectroscopy, J. Am. Chem. Soc., 139, 12773–12783, DOI: 10.1021/jacs.7b07207,
486 2017.
487 Eom, H. J., Gupta, D., Li, X., Jung, H. J., Kim, H., and Ro, C. U.: Influence of collecting substrates on
488 the characterization of hygroscopic properties of inorganic aerosol particles, Anal. Chem., 86,
489 2648–2656, DOI: 10.1021/ac4042075, 2014.
490 Fraund, M., Bonanno, D. J., China, S., Pham, D. Q., Veghte, D., Weis, J., Kulkarni, G., Teske, K.,
491 Gilles, M. K., Laskin, A., and Moffet, R. C.: Optical properties and composition of viscous
492 organic particles found in the Southern Great Plains, Atmos. Chem. Phys., 20, 11593–11606, DOI:
493 10.5194/acp-20-11593-2020, 2020.
494 Freedman, M. A.: Phase separation in organic aerosol, Chem. Soc. Rev., 46, 7694–7705, DOI:
495 10.1039/c6cs00783j, 2017.

https://doi.org/10.5194/egusphere-2025-2301
Preprint. Discussion started: 10 June 2025


Freedman, M. A.: Liquid-Liquid Phase Separation in Supermicrometer and Submicrometer Aerosol Particles, Acc. Chem. Res., 53, 1102–1110, DOI: 10.1021/acs.accounts.0c00093, 2020.

Fröhlich, R., Cubison, M. J., Slowik, J. G., Bukowiecki, N., Prévôt, A. S. H., Baltensperger, U., Schneider, J., Kimmel, J. R., Gonin, M., Rohner, U., Worsnop, D. R., and Jayne, J. T.: The ToF-ACSM: a portable aerosol chemical speciation monitor with TOFMS detection, Atmos. Meas. Tech., 6, 3225–3241, 10.5194/amt-6-3225-2013, 2013.

George, C., Ammann, M., D'Anna, B., Donaldson, D. J., and Nizkorodov, S. A.: Heterogeneous Photochemistry in the Atmosphere, Chem. Rev., 115, 4218–4258, DOI: 10.1021/cr500648z, 2015.

George, I. J. and Abbatt, J. P. D.: Heterogeneous oxidation of atmospheric aerosol particles by gas-phase radicalsm, Nat. Chem., 2, 713–722, DOI: 10.1038/nchem.806, 2010.

Ghorai, S. and Tivanski, A. V.: Hygroscopic Behavior of Individual Submicrometer Particles Studied by X-ray Spectromicroscopy, Anal. Chem., 82, 9289–9298, DOI: 10.1021/ac101797k, 2010.

Hopkins, R. J., Tivanski, A. V., Marten, B. D., and Gilles, M. K.: Chemical bonding and structure of black carbon reference materials and individual carbonaceous atmospheric aerosols, J. Aerosol Sci., 38, 573–591, DOI: 10.1016/j.jaerosci.2007.03.009, 2007.

Huthwelker, T., Zelenay, V., Birrer, M., Krepelova, A., Raabe, J., Tzvetkov, G., Vernooij, M. G. C., and Ammann, M.: An in situ cell to study phase transitions in individual aerosol particles on a substrate using scanning transmission x-ray microspectroscopy, Rev. Sci. Instrum., 81, 113706, DOI: 10.1063/1.3494604, 2010.

Jahl, L. G., Bowers, B. B., Jahn, L. G., Thornton, J. A., and Sullivan, R. C.: Response of the reaction probability of $N_2O_5$ with authentic biomass-burning aerosol to high relative humidity, ACS Earth Space Chem., 5, 2587–2598, DOI: 10.1021/acsearthspacechem.1c00227, 2021.

Jahn, L. G., Jahl, L. G., Bowers, B. B., and Sullivan, R. C.: Morphology of organic carbon coatings on biomass-burning particles and their role in reactive gas uptake, ACS Earth Space Chem., 5, 2184–2195, DOI: 10.1021/acsearthspacechem.1c00237, 2021.

Knopf, D. A., Wang, P. W., Wong, B. Y., Tomlin, J. M., Veghte, D. P., Lata, N. N., China, S., Laskin, A., Moffet, R. C., Aller, J. Y., Marcus, M. A., and Wang, J.: Physicochemical characterization of free troposphere and marine boundary layer ice-nucleating particles collected by aircraft in the eastern North Atlantic, Atmos. Chem. Phys., 23, 8659–8681, DOI: 10.5194/acp-23-8659-2023, 2023.

https://doi.org/10.5194/egusphere-2025-2301
Preprint. Discussion started: 10 June 2025


526 Kolb, C. E., Cox, R. A., Abbatt, J. P. D., Ammann, M., Davis, E. J., Donaldson, D. J., Garrett, B. C.,
527 George, C., Griffiths, P. T., Hanson, D. R., Kulmala, M., McFiggans, G., Pöschl, U., Riipinen, I.,
528 Rossi, M. J., Rudich, Y., Wagner, P. E., Winkler, P. M., Worsnop, D. R., and O'Dowd, C. D.: An
529 overview of current issues in the uptake of atmospheric trace gases by aerosols and clouds, Atmos.
530 Chem. Phys., 10, 10561–10605, DOI: 10.5194/acp-10-10561-2010, 2010.
531 Krieger, U. K., Marcolli, C., and Reid, J. P.: Exploring the complexity of aerosol particle properties
532 and processes using single particle techniques, Chem. Soc. Rev., 41, 6631–6662, DOI:
533 10.1039/c2cs35082c, 2012.
534 Lata, N. N., Zhang, B., Schum, S., Mazzoleni, L., Brimberry, R., Marcus, M. A., Cantrell, W. H.,
535 Fialho, P., Mazzoleni, C., and China, S.: Aerosol Composition, Mixing State, and Phase State of
536 Free Tropospheric Particles and Their Role in Ice Cloud Formation, ACS Earth Space Chem., 5,
537 3499–3510, DOI: 10.1021/acsearthspacechem.1c00315, 2021.
538 Latham, K. G., Simone, M. I., Dose, W. M., Allen, J. A., and Donne, S. W.: Synchrotron based
539 NEXAFS study on nitrogen doped hydrothermal carbon: Insights into surface functionalities and
540 formation mechanisms, Carbon, 114, 566–578, DOI: 10.1016/j.carbon.2016.12.057, 2017.
541 Leinweber, P., Kruse, J., Walley, F. L., Gillespie, A., Eckhardt, K. U., Blyth, R. I. R., and Regier, T.:
542 Nitrogen K-edge XANES - An overview of reference compounds used to identify 'unknown'
543 organic nitrogen in environmental samples, J. Synchrotron Radiat., 14, 500–511, DOI:
544 10.1107/s0909049507042513, 2007.
545 Li, W. J., Shao, L. Y., Zhang, D. Z., Ro, C. U., Hu, M., Bi, X. H., Geng, H., Matsuki, A., Niu, H. Y.,
546 and Chen, J. M.: A review of single aerosol particle studies in the atmosphere of East Asia:
547 morphology, mixing state, source, and heterogeneous reactions, J. Cleaner Prod., 112, 1330–1349,
548 DOI: 10.1016/j.jclepro.2015.04.050, 2016.
549 Li, W. J., Liu, L., Zhang, J., Xu, L., Wang, Y. Y., Sun, Y. L., and Shi, Z. B.: Microscopic Evidence for
550 Phase Separation of Organic Species and Inorganic Salts in Fine Ambient Aerosol Particles,
551 Environ. Sci. Technol., 55, 2234–2242, DOI: 10.1021/acs.est.0c02333, 2021.
552 Martin, S. T.: Phase transitions of aqueous atmospheric particles, Chem. Rev., 100, 3403–3453, DOI:
553 10.1021/cr990034t, 2001.
554 McCormick, R. A. and Ludwig, J. H.: Climate Modification by Atmospheric Aerosols, Science, 156,
555 1358–1359, DOI: 10.1126/science.156.3780.1358, 1967.

https://doi.org/10.5194/egusphere-2025-2301
Preprint. Discussion started: 10 June 2025


556 Middlebrook, A. M., Bahreini, R., Jimenez, J. L., and Canagaratna, M. R.: Evaluation of
557 Composition-Dependent Collection Efficiencies for the Aerodyne Aerosol Mass Spectrometer
558 using Field Data, Aerosol Sci. Technol., 46, 258–271, 10.1080/02786826.2011.620041, 2012.
559 Mikhailov, E. F., Mironov, G. N., Pöhlker, C., Chi, X., Krüger, M. L., Shiraiwa, M., Förster, J. D.,
560 Pöschl, U., Vlasenko, S. S., Ryshkevich, T. I., Weigand, M., Kilcoyne, A. L. D., and Andreae, M.
561 O.: Chemical composition, microstructure, and hygroscopic properties of aerosol particles at the
562 Zotino Tall Tower Observatory (ZOTTO), Siberia, during a summer campaign, Atmos. Chem.
563 Phys., 15, 8847–8869, DOI: 10.5194/acp-15-8847-2015, 2015.
564 Moffet, R. C., Henn, T., Laskin, A., and Gilles, M. K.: Automated Chemical Analysis of Internally
565 Mixed Aerosol Particles Using X-ray Spectromicroscopy at the Carbon K-Edge, Anal. Chem., 82,
566 7906–7914, DOI: 10.1021/ac1012909, 2010a.
567 Moffet, R. C., Henn, T. R., Tivanski, A. V., Hopkins, R. J., Desyaterik, Y., Kilcoyne, A. L. D.,
568 Tyliszczak, T., Fast, J., Barnard, J., Shutthanandan, V., Cliff, S. S., Perry, K. D., Laskin, A., and
569 Gilles, M. K.: Microscopic characterization of carbonaceous aerosol particle aging in the outflow
570 from Mexico City, Atmos. Chem. Phys., 10, 961–976, DOI: 10.5194/acp-10-961-2010, 2010b.
571 Moffet, R. C., Tivanski A. V., and Gilles M. K.: Scanning Transmission X-ray Microscopy
572 Applications in Atmospheric Aerosol Research, Fundamentals and Applications in Aerosol
573 Spectroscopy, edited by: Signorell, R., and Reid, J. P., CRC Press, the U.S., 419–462, ISBN:
574 9781420085617, 2011.
575 Moffet, R. C., Rödel, T. C., Kelly, S. T., Yu, X. Y., Carroll, G. T., Fast, J., Zaveri, R. A., Laskin, A.,
576 and Gilles, M. K.: Spectro-microscopic measurements of carbonaceous aerosol aging in Central
577 California, Atmos. Chem. Phys., 13, 10445–10459, DOI: 10.5194/acp-13-10445-2013, 2013.
578 Moffet, R. C., O'Brien, R. E., Alpert, P. A., Kelly, S. T., Pham, D. Q., Gilles, M. K., Knopf, D. A., and
579 Laskin, A.: Morphology and mixing of black carbon particles collected in central California
580 during the CARES field study, Atmos. Chem. Phys., 16, 14515–14525, DOI:
581 10.5194/acp-16-14515-2016, 2016.
582 Noll, K. E., Mueller, P. K., and Imada, M.: Visibility and aerosol concentration in urban air, Atmos.
583 Environ., 2, 465–475, DOI: 10.1016/0004-6981(68)90040-1, 1968.

https://doi.org/10.5194/egusphere-2025-2301
Preprint. Discussion started: 10 June 2025


584 O'Brien, R. E., Wang, B. B., Kelly, S. T., Lundt, N., You, Y., Bertram, A. K., Leone, S. R., Laskin, A.,
585 and Gilles, M. K.: Liquid-Liquid Phase Separation in Aerosol Particles: Imaging at the Nanometer
586 Scale, Environ. Sci. Technol., 49, 4995–5002, DOI: 10.1021/acs.est.5b00062, 2015.
587 Peng, C., Chen, L. X. D., and Tang, M. J.: A database for deliquescence and efflorescence relative
588 humidities of compounds with atmospheric relevance, Fundam. Res., 2, 578–587, DOI:
589 10.1016/j.fmre.2021.11.021, 2022.
590 Penner, J. E. and Novakov, T.: Carbonaceous particles in the atmosphere: A historical perspective to
591 the Fifth International Conference on Carbonaceous Particles in the Atmosphere, J. Geophys. Res.:
592 Atmos., 101, 19373–19378, DOI: 10.1029/96JD01175, 1996.
593 Piens, D. S., Kelly, S. T., Harder, T. H., Petters, M. D., O'Brien, R. E., Wang, B. B., Teske, K., Dowell,
594 P., Laskin, A., and Gilles, M. K.: Measuring Mass-Based Hygroscopicity of Atmospheric Particles
595 through in Situ Imaging, Environ. Sci. Technol., 50, 5172–5180, DOI: 10.1021/acs.est.6b00793,
596 2016.
597 Pöhlker, C., Saturno, J., Krüger, M. L., Förster, J. D., Weigand, M., Wiedemann, K. T., Bechtel, M.,
598 Artaxo, P., and Andreae, M. O.: Efflorescence upon humidification? X-ray microspectroscopic in
599 situ observation of changes in aerosol microstructure and phase state upon hydration, Geophys.
600 Res. Lett., 41, 3681–3689. DOI: 10.1002/2014gl059409, 2014.
601 Prather, K. A., Bertram, T. H., Grassian, V. H., Deane, G. B., Stokes, M. D., DeMott, P. J., Aluwihare,
602 L. I., Palenik, B. P., Azam, F., Seinfeld, J. H., Moffet, R. C., Molina, M. J., Cappa, C. D., Geiger,
603 F. M., Roberts, G. C., Russell, L. M., Ault, A. P., Baltrusaitis, J., Collins, D. B., Corrigan, C. E.,
604 Cuadra-Rodriguez, L. A., Ebben, C. J., Forestieri, S. D., Guasco, T. L., Hersey, S. P., Kim, M. J.,
605 Lambert, W. F., Modini, R. L., Mui, W., Pedler, B. E., Ruppel, M. J., Ryder, O. S., Schoepp, N.
606 G., Sullivan, R. C., and Zhao, D. F.: Bringing the ocean into the laboratory to probe the chemical
607 complexity of sea spray aerosol, Proc. Natl. Acad. Sci. U. S. A., 110, 7550–7555, DOI:
608 10.1073/pnas.1300262110, 2013.
609 Raabe, J., Tzvetkov, G., Flechsig, U., Böge, M., Jaggi, A., Sarafimov, B., Vernooij, M. G. C.,
610 Huthwelker, T., Ade, H., Kilcoyne, D., Tyliszczak, T., Fink, R. H., and Quitmann, C.: PolLux: A
611 new facility for soft x-ray spectromicroscopy at the Swiss Light Source, Rev. Sci. Instrum., 79,
612 113704, DOI: 10.1063/1.3021472, 2008.

https://doi.org/10.5194/egusphere-2025-2301
Preprint. Discussion started: 10 June 2025


613 Rasool, S. I. and Schneider, S. H.: Atmospheric Carbon Dioxide and Aerosols: Effects of Large
614 Increases on Global Climate, Science, 173, 138–141, DOI: 10.1126/science.173.3992.138, 1971.
615 Reynolds, R. S. and Wilson, K. R.: Unraveling the Meaning of Effective Uptake Coefficients in
616 Multiphase and Aerosol Chemistry, Acc. Chem. Res., 58, 366–374, 10.1021/acs.accounts.4c00662,
617 2025.
618 Riemer, N., Ault, A. P., West, M., Craig, R. L., and Curtis, J. H.: Aerosol Mixing State: Measurements,
619 Modeling, and Impacts, Rev. Geophys., 57, 187–249, DOI: 10.1029/2018rg000615, 2019.
620 Shao, L. Y., Liu, P. J., Jones, T., Yang, S. S., Wang, W. H., Zhang, D. Z., Li, Y. W., Yang, C.-X., Xing,
621 J. P., Hou, C., Zhang, M. Y., Feng, X. L., Li, W. J., and BéruBé K.: A review of atmospheric
622 individual particle analyses: Methodologies and applications in environmental research,
623 Gondwana Res., 110, 347–369, DOI: 10.1016/j.gr.2022.01.007, 2022.
624 Slowik, J. G., Cziczo, D. J., and Abbatt, J. P. D.: Analysis of cloud condensation nuclei composition
625 and growth kinetics using a pumped counterflow virtual impactor and aerosol mass spectrometer,
626 Atmos. Meas. Tech., 4, 1677–1688, DOI: 10.5194/amt-4-1677-2011, 2011.
627 Smith, J. W., Lam, R. K., Shih, O., Rizzuto, A. M., Prendergast, D., and Saykally, R. J.: Properties of
628 aqueous nitrate and nitrite from x-ray absorption spectroscopy, J. Chem. Phys., 143, 084503, DOI:
629 10.1063/1.4928867, 2015.
630 Stokes, R. H. and Robinson, R. A.: Interactions in aqueous nonelectrolyte solutions. I. Solute-solvent
631 equilibria, J. Phys. Chem., 70, 2126–2131, DOI: 10.1021/j100879a010, 1966.
632 Su, H., Cheng, Y. F., and Pöschl, U.: New Multiphase Chemical Processes Influencing Atmospheric
633 Aerosols, Air Quality, and Climate in the Anthropocene, Acc. Chem. Res., 53, 2034–2043, DOI:
634 10.1021/acs.accounts.0c00246, 2020.
635 Tang, L. Z., Shang, D. J., Fang, X., Wu, Z. J., Qiu, Y. T., Chen, S. Y., Li, X., Zeng, L. M., Guo, S., and
636 Hu, M.: More Significant Impacts From New Particle Formation on Haze Formation During
637 COVID-19 Lockdown, Geophys. Res. Lett., 48, e2020GL091591, 10.1029/2020gl091591, 2021.
638 Tang, M. J., Cziczo, D. J., and Grassian, V. H.: Interactions of Water with Mineral Dust Aerosol:
639 Water Adsorption, Hygroscopicity, Cloud Condensation, and Ice Nucleation, Chem. Rev., 116,
640 4205–4259, DOI: 10.1021/acs.chemrev.5b00529, 2016.

https://doi.org/10.5194/egusphere-2025-2301
Preprint. Discussion started: 10 June 2025


641 Tang, M. J., Chan, C. K., Li, Y. J., Su, H., Ma, Q. X., Wu, Z. J., Zhang, G. H., Wang, Z., Ge, M. F., Hu,
642 M., He, H., and Wang, X. M.: A review of experimental techniques for aerosol hygroscopicity
643 studies, Atmos. Chem. Phys., 19, 12631–12686, DOI: 10.5194/acp-19-12631-2019, 2019.
644 Tomlin, J. M., Weis, J., Veghte, D. P., China, S., Fraund, M., He, Q., Reicher, N., Li, C., Jankowski, K.
645 A., Rivera-Adorno, F. A., Morales, A. C., Rudich, Y., Moffet, R. C., Gilles, M. K., and Laskin, A.:
646 Chemical composition and morphological analysis of atmospheric particles from an intensive
647 bonfire burning festival, Environ. Sci.: Atmos., 2, 616–633, DOI: 10.1039/d2ea00037g, 2022.
648 Ulbrich, I. M., Canagaratna, M. R., Zhang, Q., Worsnop, D. R., and Jimenez, J. L.: Interpretation of
649 organic components from Positive Matrix Factorization of aerosol mass spectrometric data, Atmos.
650 Chem. Phys., 9, 2891–2918, DOI: 10.5194/acp-9-2891-2009, 2009.
651 Wagner, N. L., Riedel, T. P., Young, C. J., Bahreini, R., Brock, C. A., Dubé, W. P., Kim, S.,
652 Middlebrook, A. M., Öztürk, F., Roberts, J. M., Russo, R., Sive, B., Swarthout, R., Thornton, J. A.,
653 VandenBoer, T. C., Zhou, Y., and Brown, S. S.: $N_2O_5$ uptake coefficients and nocturnal $NO_2$
654 removal rates determined from ambient wintertime measurements, J. Geophys. Res.: Atmos., 118,
655 9331–9350, DOI: 10.1002/jgrd.50653, 2013.
656 Warwick, T., Franck, K., Kortright, J. B., Meigs, G., Moronne, M., Myneni, S., Rotenberg, E., Seal, S.,
657 Steele, W. F., Ade, H., Garcia, A., Cerasari, S., Delinger, J., Hayakawa, S., Hitchcock, A. P.,
658 Tyliszczak, T., Kikuma, J., Rightor, E. G., Shin, H. J., and Tonner, B. P.: A scanning transmission
659 x-ray microscope for materials science spectromicroscopy at the advanced light source, Rev. Sci.
660 Instrum., 69, 2964–2973, DOI: 10.1063/1.1149041, 1998.
661 Wu, L. and Ro, C. U.: Aerosol Hygroscopicity on A Single Particle Level Using Microscopic and
662 Spectroscopic Techniques: A Review, Asian J. Atmos. Environ., 14, 177–209, DOI:
663 10.5572/ajae.2020.14.3.177, 2020.
664 Wu, Z. J., Hu, M., Liu, S., Wehner, B., Bauer, S., Ma ßling, A., Wiedensohler, A., Petäjä, T., Dal Maso,
665 M., and Kulmala, M.: New particle formation in Beijing, China: Statistical analysis of a 1-year
666 data set, J. Geophys. Res.: Atmos., 112, D0920, 10.1029/2006jd007406, 2007.
667 Wu, Z. J., Zheng, J., Shang, D. J., Du, Z. F., Wu, Y. S., Zeng, L. M., Wiedensohler, A., and Hu, M.:
668 Particle hygroscopicity and its link to chemical composition in the urban atmosphere of Beijing,
669 China, during summertime, Atmos. Chem. Phys., 16, 1123–1138, DOI:
670 10.5194/acp-16-1123-2016, 2016.

https://doi.org/10.5194/egusphere-2025-2301
Preprint. Discussion started: 10 June 2025


671 Wu, Z. J., Zheng, J., Wang, Y., Shang, D. J., Du, Z. F., Zhang, Y. H., and Hu, M.: Chemical and
672 physical properties of biomass burning aerosols and their CCN activity: A case study in Beijing,
673 China, Sci. Total Environ., 579, 1260–1268, DOI: 10.1016/j.scitotenv.2016.11.112, 2017.
674 Xiao, Z. M., Xu, H., Gao, J. Y., Cai, Z. Y., Bi, W. K., Li, P., Yang, N., Deng, X. W., Ji, Y. F.:
675 Characteristics and Sources of $PM_{2.5}$-$O_3$ Compound Pollution in Tianjin, Environmental Science
676 (Chinese), 43, 1140–1150, DOI: 10.13227/j.hjkx.202108164, 2022.
677 You, Y., Renbaum-Wolff, L., Carreras-Sospedra, M., Hanna, S. J., Hiranuma, N., Kamal, S., Smith, M.
678 L., Zhang, X. L., Weber, R. J., Shilling, J. E., Dabdub, D., Martin, S. T., and Bertram, A. K.:
679 Images reveal that atmospheric particles can undergo liquid-liquid phase separations, Proc. Natl.
680 Acad. Sci. U. S. A., 109, 13188–13193, DOI: 10.1073/pnas.1206414109, 2012.
681 You, Y., Renbaum-Wolff, L., and Bertram, A. K.: Liquid-liquid phase separation in particles
682 containing organics mixed with ammonium sulfate, ammonium bisulfate, ammonium nitrate or
683 sodium chloride, Atmos. Chem. Phys., 13, 11723–11734, DOI: 10.5194/acp-13-11723-2013,
684 2013.
685 You, Y., Smith, M. L., Song, M. J., Martin, S. T., and Bertram, A. K.: Liquid–liquid phase separation
686 in atmospherically relevant particles consisting of organic species and inorganic salts, Int. Rev.
687 Phys. Chem., 33, 43–77, DOI: 10.1080/0144235x.2014.890786, 2014.
688 Yu, X., Li, Q. F., Liao, K. Z., Li, Y. M., Wang, X. M., Zhou, Y., Liang, Y. M., and Yu, J. Z.: New
689 measurements reveal a large contribution of nitrogenous molecules to ambient organic aerosol, npj
690 Clim. Atmos. Sci., 7, 72, DOI: 10.1038/s41612-024-00620-6, 2024.
691 Zelenay, V., Ammann, M., Křepelová, A., Birrer, M., Tzvetkov, G., Vernooij, M. G. C., Raabe, J., and
692 Huthwelker, T.: Direct observation of water uptake and release in individual submicrometer sized
693 ammonium sulfate and ammonium sulfate/adipic acid particles using X-ray microspectroscopy, J.
694 Aerosol Sci., 42, 38–51, DOI: 10.1016/j.jaerosci.2010.11.001, 2011a.
695 Zelenay, V., Huthwelker, T., Krepelová, A., Rudich, Y., and Ammann, M.: Humidity driven nanoscale
696 chemical separation in complex organic matter, Environ. Chem., 8, 450–460, DOI:
697 10.1071/en11047, 2011b.
698 Zhang, J., Wang, Y. Y., Teng, X. M., Liu, L., Xu, Y. S., Ren, L. H., Shi, Z. B., Zhang, Y., Jiang, J. K.,
699 Liu, D. T., Hu, M., Shao, L. Y., Chen, J. M., Martin, S. T., Zhang, X. Y., and Li, W. J.:

https://doi.org/10.5194/egusphere-2025-2301
Preprint. Discussion started: 10 June 2025


Liquid-liquid phase separation reduces radiative absorption by aged black carbon aerosols, Commun. Earth Environ., 3, 128, DOI: 10.1038/s43247-022-00462-1, 2022.

Zheng, Y., Cheng, X., Liao, K. R., Li, Y. W., Li, Y. J., Huang, R.-J., Hu, W. W., Liu, Y., Zhu, T., Chen, S. Y., Zeng, L. M., Worsnop, D. R., and Chen, Q.: Characterization of anthropogenic organic aerosols by TOF-ACSM with the new capture vaporizer, Atmos. Meas. Tech., 13, 2457–2472, 10.5194/amt-13-2457-2020, 2020.

Zheng, Y., Miao, R. Q., Zhang, Q., Li, Y. W., Cheng, X., Liao, K. R., Koenig, T. K., Ge, Y. L., Tang, L. Z., Shang, D. J., Hu, M., Chen, S. Y., and Chen, Q.: Secondary Formation of Submicron and Supermicron Organic and Inorganic Aerosols in a Highly Polluted Urban Area, J. Geophys. Res.: Atmos., 128, e2022JD037865, 10.1029/2022jd037865, 2023.

Ziemann, P. J. and Atkinson, R.: Kinetics, products, and mechanisms of secondary organic aerosol formation, Chem. Soc. Rev., 41, 6582–6605, DOI: 10.1039/c2cs35122f, 2012.

Zong, T. M., Wang, H. C., Wu, Z. J., Lu, K. D., Wang, Y., Zhu, Y. S., Shang, D. J., Fang, X., Huang, X. F., He, L. Y., Ma, N., Grösss, J., Huang, S., Guo, S., Zeng, L. M., Herrmann, H., Wiedensohler, A., Zhang, Y. H., and Hu, M.: Particle hygroscopicity inhomogeneity and its impact on reactive uptake, Sci. Total Environ., 811, 151364, DOI: 10.1016/j.scitotenv.2021.151364, 2022.